Received: 25 April 2017 | Accepted: 21 June 2017

DOI: 10.1111/jace.15052

ORIGINAL ARTICLE

Journal of the American Ceramic Society

Determination of heat conductivity of waste glass feed and its applicability for modeling the batch-to-glass conversion

Miroslava Hujova[1] | Richard Pokorny[1] | Jaroslav Klouzek[1] | Derek R. Dixon[2] | Derek A. Cutforth[2] | Seungmin Lee[2] | Benjamin P. McCarthy[2] | Michael J. Schweiger[2] | Albert A. Kruger[3] | Pavel Hrma[2]

[1]Laboratory of Inorganic Materials, Joint Workplace of the University of Chemistry and Technology Prague and the Institute , Institute of Rock Structure and Mechanics of the ASCR, Prague, Czech Republic

[2]Radiological Materials & Detection Group, Pacific Northwest National Laboratory, Richland, Washington

[3]U.S. Department of Energy, Office of River Protection, Richland, Washington

Correspondence
Richard Pokorny, Laboratory of Inorganic Materials, Joint Workplace of the University of Chemistry and Technology, Prague, Czech Republic.
Email: richard.pokorny@vscht.cz

Funding information
Department of Energy's Waste Treatment and Immobilization Plant Federal Project Office; MSMT, Grant/Award Number: 20-SVV/2017

Abstract

The effective heat conductivity (λ) of reacting melter feed affects the heat transfer and conversion process in the cold cap, a layer of reacting feed floating on molten glass. A heat conductivity meter was used to measure λ of samples of a cold cap retrieved from a laboratory-scale melter, loose dry powder feed samples, and samples cut from fast-dried slurry blocks. These blocks were formed to simulate the feed conditions in the cold-cap by rapidly evaporating water from feed slurry poured onto a 200°C surface. Our study indicates that the effective heat conductivity of the feed in the cold cap is significantly higher than that of loose dry powder feed, which is a result of the feed solidification during the water evaporation from the feed slurry. To assess the heat transfer at higher temperatures when feed turns into foam, we developed a theoretical model that predicts the foam heat conductivity based on morphology data from in-situ X-ray computed tomography. The implications for the mathematical modeling of the cold cap are discussed.

KEYWORDS
foams, glassmelting, modeling/model, thermal conductivity

1 | INTRODUCTION

The Hanford Waste Treatment and Immobilization Plant is tasked to immobilize radioactive waste from plutonium production in the form of stable glass[1]. This glass will be formed by melting radioactive waste mixed with glass-forming and glass-modifying additives in an all-electric Joule-heated melter. When poured into the melter, the melter feed creates a cold cap, a layer of reacting feed components floating on the surface of molten glass (Figure 1). The cold cap consists of two main layers: the open-porosity layer and, below it, the foam layer that contains gas bubbles trapped in glass-forming melt. Although most of the gas-evolving reactions take place in the upper layer before open porosity closes at foam onset temperature T_{FO}, the residual gases evolving at $T>T_{FO}$ are responsible for the evolution of primary foam.[2] At even higher temperatures, the decreasing melt viscosity allows bubbles to coalesce and foam to collapse; convective currents then sweep away large bubbles to cold cap edges or to vent holes where they escape to the plenum space.

Batch melting in a cold cap is assumed to be jointly controlled by the heat transfer from the pool of molten glass and by the batch-to-glass conversion kinetics. Thus, behavior and properties of the cold cap have been the subject of numerous experimental and modeling studies.[3-10] This study focuses on the determination of the effective heat conductivity (λ) of the cold cap, which greatly affects the heat transfer,[11,12] and thus has a strong impact on the rate of melting, temperature profile, and other phenomena,

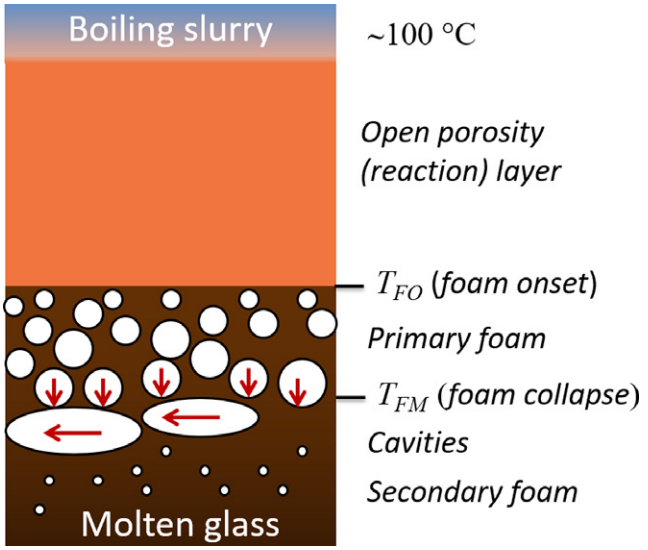

FIGURE 1 Schematic Illustration of a cold cap displaying typical cold cap layers

such as silica dissolution or spinel formation. Having a realistic $\lambda(T)$ function, which depends on the effective conductivities of individual phases, including thermal radiation, and on the 3D morphology, is crucial for the development of the advanced cold-cap model.[12]

In our previous work,[11,13] we followed studies of Faber,[14] Conradt,[15] and Verheijen,[16,17] and obtained the λ values from measured temperature profiles in a cylindrical crucible filled with a powdered simulated nuclear waste feed. The crucible wall was heated at a constant rate from room temperature up to 1100°C.[11,13] Although this experimental setup provided a reasonable estimate of the heat conductivity for use in the recently developed mathematical model of the cold cap,[12,18] it also has several drawbacks. The small number and wide spacing of the thermocouples in this setup result in a high uncertainty of heat conductivity values calculated from the dynamic experiment.[16] Also, the temperatures measured by thermocouples are affected by (i) the reaction heat, (ii) the flow of gases from gas-evolving reactions, and (iii) the feed movement during compaction and foaming. Last, the heat conductivity was obtained for feed samples in the form of loose, dry powder, whereas the structure of the feed in an actual cold cap, which is formed by water evaporation from the feed slurry, is rigid, resembling porous rock.

To address these issues and validate our previous results, we measured λ of loose dry powder feed at various levels of compaction (densities) using the transient hot bridge method (THB).[19] Further, we prepared "fast-dried slurry blocks" (FDSBs) by evaporating water from the feed slurry to simulate the conditions during the cold-cap formation. Finally, we measured the heat conductivity of actual cold-cap samples retrieved from a laboratory-scale melter (LSM), obtaining a good agreement with the FDSB values.

The disadvantage of the THB method is that the λ measurement is limited to room temperature. Thus, it is inadequate for samples whose structure (and thus λ) significantly changes upon cooling, such as for samples containing primary foam. Instead, we present a theoretical model for the heat conductivity of primary foam that employs the foam morphology data obtained from X-ray computed tomography[2] (porosity and bubble size), together with literature models for multiphase heat transfer, including radiation.[20,21] The results are in reasonable agreement with λ values reported for primary foam. Having such a model is invaluable for the development of the cold-cap mathematical model, since the measurement of heat conductivity is subject to high uncertainty once the feed starts to move during its shrinkage and primary foaming.

2 | THEORY

2.1 | Heat conductivity of multiphase materials

Many analytical equations exist regarding the estimation of effective heat conductivity of porous or hetero-phase materials, such as solid mixtures or glass foams. Generally, the heat conductivity of such materials depends both on the effective conductivities of individual phases, including thermal radiation, and on the 3D arrangement of the solid/liquid mixture. Frequently used analytical equations are based on the parallel plates model, the series plates model, the effective medium theory model, the Maxwell model, the Hamilton model, and the reciprocity model.[20]

The disadvantage of these analytical models is that they consider simple predefined morphology. For example, the effective medium theory model considers only materials with a completely random distribution of all components. The Maxwell model is valid for a dispersion of small particles within a continuous matrix phase in which the particles are far apart from each other, so that the local distortions of the transport characteristics around each particle do not interfere with those of their neighbors.[15] Thus, several approaches were proposed to expand the applicability of the analytical models. One commonly used route is to treat the heterogeneous material as a combination of parallel and series resistors, whose effective heat conductivity can be calculated as a weighted mean.[16,20]

In addition to analytical models, many empirical or semi-empirical equations have been developed for more complicated morphologies. Empirical coefficients in these equations are obtained by numerical fitting to experimental data.[20,22-24] Although this approach is useful in specific cases, it is limited by the limited validity of empirical parameters.

With the rapidly increasing computer power, the focus is shifting to development of accurate numerical methodology. Contrary to empirical models, numerical simulations do not

use empirical parameters and are successfully used for material morphology optimization or even for the design of new materials.[25,26] The common approach employs the 2D or 3D computer reconstruction of real materials using microscopy or tomography images and its discretization into 2D or 3D mesh, and subsequent simulation of the heat transfer using a suitable method, such as the finite volume method (FVM), finite element method, or lattice Boltzmann method. One of the critical issues with this approach is often, as is the case in our work as well, the quality of the microscopy or tomography images, which often do not capture the morphology in sufficient detail.[27]

2.2 | Heat conductivity of condensed phase

One of the main components of reacting waste batch feed is crystalline silica. Its phonon conductivity is limited by scattering of the phonons at lattice imperfections. This scattering generally increases with increasing temperature; therefore, the phonon conductivity of crystalline silica decreases with increasing temperature, from 273 to 1373 K, according to Verheijen:[16]

$$\lambda_{\text{silica}} = 2.81 + 8.60 \times 10^2 T^{-1} + 2.11 \times 10^5 T^{-2}, \quad (1)$$

where T is temperature in K and λ is in $\text{W}\cdot\text{m}^{-1}\cdot\text{K}^{-1}$.

In the case of amorphous components, such as glasses or melts, where no short-range structural ordering of atoms is present, the phononic heat conductivity is generally much lower than that in crystalline materials. Thermal dependence of phononic heat conductivity is mainly given by the thermal dependence of the specific heat of the species. For example, Mann et al.[28] measured the intrinsic phonon conductivity of float glass up to about 780 K, which is given by

$$\lambda_{\text{float\_glass}} = 0.97 + 6.24 \times 10^{-4} T. \quad (2)$$

In this study, the components of a waste glass batch are both crystalline and amorphous, and therefore the temperature of the mixture is considered to have only a negligible effect on heat conductivity up to 700°C, which agrees with our previous experimental results.[11,13] Above this temperature, the feed structure changes as the primary melt and foam appears, and λ starts to change significantly.

2.3 | Heat conductivity of gas phase

The temperature-dependent heat conductivity of air up to 1300 K is[29]

$$\lambda_{\text{G\_cond}} = 1.2 \times 10^{-2} + 5.5 \times 10^{-5} T \quad (3)$$

At higher temperatures, when the glass batch turns into primary foam and the pores become spherical, the contribution of radiation must be also considered. According to Loeb,[21] the radiative contribution to heat conductivity, $\lambda_{\text{G\_rad}}$, is given by

$$\lambda_{\text{G\_rad}} = 4\gamma d\varepsilon\sigma T^3 \quad (4)$$

where γ is the shape factor (γ=2/3 for spherical pores), d is the pore diameter, ε is the emissivity, and σ is the Stefan-Boltzmann constant. For molten glass, ε=0.88, taken from Viskanta and Wu.[30] Equation 4 sometimes also includes the term n^2, where n is the refraction index of gas. But considering that n is close to unity for typical gases (1.000293 for air), it is often omitted. The overall gas effective heat conductivity is then $\lambda_G=\lambda_{G\_cond}+\lambda_{G\_rad}$. Keep in mind that Equation 4 can be used only for opaque glass in which the interface directly absorbs radiation. A more complex model that considers spectral absorption coefficient, extinction coefficients, and single scattering albedo is needed for semi-transparent media containing large gas bubbles.[31,32]

2.4 | Heat conductivity of porous glass batch

Verheijen[16] tested several methods to estimate the heat conductivity of a silica sand and soda-lime-silica batch from room temperature up to 1000°C. He concluded that none of the simple models, such as series or parallel plates models, a continuous phase network model (CPNM), or a dispersed phase network model (DPNM), predicted the temperature-dependent heat conductivity that would be close to experimentally measured data. Instead, he obtained an excellent agreement with measured data with a weighted mean of series and parallel resistances, given by

$$\lambda_{\text{T\_eff}} = 1/(\psi/\lambda_{\text{PNM}} + (1-\psi)/\lambda_{\text{SNM}}) \quad (5)$$

where Ψ is the connectivity parameter, $\lambda_{SNM}=\varepsilon_G\lambda_G+(1-\varepsilon_G)\lambda_S$, and $\lambda_{PNM}=1/(\varepsilon_G/\lambda_G+(1-\varepsilon_G)/\lambda_S)$, λ_S and λ_G are the heat conductivities of the condensed and gas phases, respectively, and ε_G is porosity. In his work, he obtained Ψ=0.29 by fitting Equation 5 to measured data for silica sand. In our work, ε_G will be evaluated from in-situ X-ray computed tomography (CT).

3 | EXPERIMENTAL

3.1 | Feed preparation and heat treatment

3.1.1 | Dry melter feed powder

The powder batches were prepared as is described in Schweiger et al.[9] The compositions of two high-alumina high-level waste melter feeds (named A0 and A19) are provided in Table 1. Both glasses are simplified versions of the glass designed for the Hanford Waste Treatment and Immobilization Plant.[33] The feed chemicals were mixed in deionized

water to prepare slurry. The slurry feed was dried at 105°C overnight in an oven and milled to powder. Samples were prepared by heating dry feed in quartz crucibles at a rate of 10 $K \cdot min^{-1}$ to test temperatures (up to 800°C), from which they were quenched in the air.

Figure 2A displays the initial state of the A19 dry feed before the heat treatment of samples for the heat conductivity measurements. During heating, the feed undergoes a significant (~20%) weight loss associated with decomposition reactions (mainly evolution of water, carbon and nitrogen oxides, and oxygen). Significant shrinkage of the feed occurs between ~700°C and ~800°C (shown in Figure 2B), caused by sintering of the feed and formation of primary and glass-forming melt. After the open porosity closes, the feed turns into foam. Table 2 summarizes the density of the A19 dry feed as a function of temperature.

TABLE 1 Composition of A0 and A19 melter feeds (in g) to make 1 kg of glass

Compound	A0 ($g \cdot kg^{-1}$)	A19 ($g \cdot kg^{-1}$)
$Al(OH)_3$	367.49	371.79
H_3BO_3	269.83	341.59
CaO	60.79	10.87
$Fe(OH)_3$	73.82	74.38
Li_2CO_3	88.30	89.22
$Mg(OH)_2$	1.69	
NaOH	99.41	19.87
SiO_2	305.05	221.45
$Zn(NO_3)_2 \cdot 4H_2O$	2.67	
$Zr(OH)_4 \cdot 0.65H_2O$	5.49	5.53
Na_2SO_4	3.55	3.60
$Bi(OH)_3$	12.80	
Bi_2O_3		11.67
$Cr_2O_3 \cdot 1.5H_2O$		6.20
Na_2CrO_4	11.13	
KNO_3	3.04	
$NiCO_3$	6.36	
$Ni(OH)_2$		5.03
$Pb(NO_3)_2$	6.08	
PbO		4.17
$Fe(H_2PO_2)_3$	12.42	12.51
NaF	14.78	15.00
Na_2CO_3		106.57
$NaNO_2$	3.37	3.48
$NaNO_3$		12.40
$Na_2C_2O_4$	1.26	1.26
$CaSiO_3$		97.07
Total	1349.32	1413.66

3.1.2 | Cold-cap sample preparation

The A19 feed slurry, prepared as described above, was batched at a glass yield of 400 $g \cdot L^{-1}$ of slurry and charged into a 9.5 cm diameter LSM vessel, at a glass production rate of 665 $kg \cdot m^{-2} \cdot day^{-1}$, as described previously by Dixon et al.[34] After charging for 35 minutes to form a cold cap, the crucible was removed from the LSM furnace and rapidly cooled. The cooling process resulted in fracturing of the cold cap from which several samples of reciprocal cold-cap surfaces were sanded as shown in Figure 2C.

3.1.3 | Fast-dried slurry blocks (FDSBs)

The FDSBs were prepared to simulate the structure of the feed material in the cold cap. Feed slurry with a glass yield of 400 $g \cdot L^{-1}$ was charged at 4.5 $mL \cdot min^{-1}$ into a 12 cm×4 cm×5 cm, aluminum-foil-lined stainless steel mold. The mold was held at 200°C on a hot plate for the duration of slurry charging. Charging stopped after 60 minutes. The remaining water boiled off within 5 minutes, after which the mold was removed from the hot plate and allowed to cool to room temperature. The dried samples were peeled away from the aluminum foil and sanded to a flat-bottomed block as shown in Figure 2D. Visual inspection of the FDSB samples revealed similar structure to the cold cap sample displayed in Figure 2C. Individual FDSBs were then heat treated to temperatures ranging from 400°C to 700°C at 5 $K \cdot min^{-1}$, which corresponds to the reacting feed region of the cold cap.

The densities of the FDSBs, listed in Table 2, are higher than that of dry feed powder in the entire temperature range below the onset of foaming. The density was evaluated by the Archimedes method in a kerosene medium and geometrically by dividing the mass of the sample by its volume, obtaining a good agreement between the two methods. The difference for the 200°C FDSB sample could be caused by the presence of closed porosity at lower temperatures, which is not captured by the Archimedes method. A small amount of closed porosity in the sample could be formed by liquid (molten salts) and amorphous (borate, alumina) phases in the sample.

A cross-sectional image of a non-heat-treated FDSB and the reacting feed region of a cold cap retrieved from the LSM, obtained from X-ray computed tomography, are shown in Figure 3. The reacting feed region in the cold cap (Figure 3B) varies in temperature from ~100°C at the top to ~700°C at the bottom where gases begin to accumulate into bubbles, while the temperature of the feed in the non-heat-treated FDSB doesn't exceed 300°C. Similar material (gray pixels) and void (black pixels) structures can be observed in both samples: (i) the red marked areas showing the top surface from which slurry evaporated last,

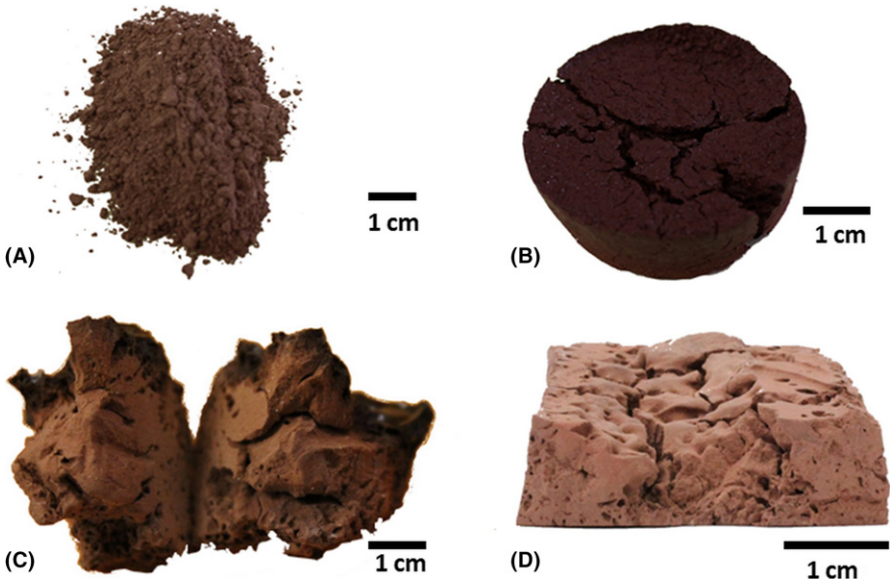

FIGURE 2 Images of A) loose feed, B) compacted feed, C) LSM cold-cap sample, and D) FDSB before heat treatment

TABLE 2 Density ($kg \cdot m^{-3}$) of A 19 dry batch and "fast-dried slurry blocks" (FDSBs) as a function of temperature. Samples were heated at 10 $K \cdot min^{-1}$. "Glassy" samples showed visible presence of glass-forming melt, and their heat conductivity likely significantly changes upon cooling as phase change occurs when the melt solidifies

Temperature	A19 dry feed	FDSB - Geometric	FDSB - Archimedes
200	1130	1550	1370
400	960	1220	1240
500	–	1120	1140
600	870	1120	1110
625	–	1060	–
650	–	1000	–
700	790	glassy	glassy
770	1430	glassy	glassy
790	1650 (glassy)	glassy	glassy
800	1760 (glassy)	glassy	glassy
>800	glassy	glassy	glassy

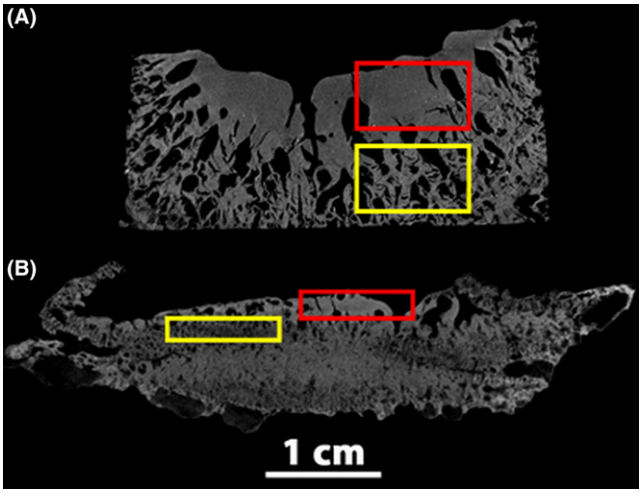

FIGURE 3 X-ray computed tomography images of A) non-heat-treated FDSB and B) the reacting feed region of a cold cap generated from the LSM. Similar structures can be observed in both samples, as illustrated by red (top surface structure) and yellow (porous region) boxes

and (ii) the yellow marked areas showing porous regions corresponding to feed temperatures between 200-300°C, in which a large amount of gases is liberated.

3.2 | Heat conductivity measurements

The heat conductivity of samples was measured using a Linseis THB-100 m. The principle of the THB method is described in detail in Hammerschmidt and Meier.[19] The probe is a thin strip shaped conductor, which is used as both the heat source and temperature sensor. During the measurement, the probe is inserted into the powder feed or sandwiched between two flat samples of solid material (in the case of FDSB or cold-cap samples).

Two types of probes were used in this study: the hot bridge sensor (THB) with a higher accuracy, but requiring larger samples (min. sample dimension 45 mm×25 mm×5 mm); and the hot point sensor (HTP, Linseis GmbH, Selb, Germany), which can measure samples as small as 3 mm×3 mm×3 mm, but has slightly lower accuracy. The sensors were calibrated using the standards provided. Each measurement was repeated at least three times and the average value was reported. The measurement accuracy was within 3%.

3.3 | Heat penetration experiment

To compare the thermal properties of A0 and A19 melter feed, a heat penetration experiment was conducted as described in our previous studies[11,13] with the A19 feed. The feed (465 g) was placed in a fused silica ceramic crucible (DFC Ceramics, Inc., Canon City, CO) 10 cm in diameter and 19 cm high; see Figure 4. Two type-K thermocouples (TCs), labeled A1 and A2, were attached to the opposite sides of the crucible external wall; two TCs, labeled B1 and B2, were attached to the inner wall; and six TCs, labeled C1, D1, E1, E2, D2, and C2, were spaced evenly through the feed at ~2.5 cm below the surface of the feed.

Figure 5 shows the comparison of the temperature field evolution in the A0 (dashed line) and A19 (solid line) melter feeds while the crucible was heated at 5 K·min^{-1} (the A0 data are taken from our previous study[11]). The A19 and A0 temperature fields follow a similar pattern: the nearly parabolic radial temperature profiles markedly changed with the time of heating, becoming nearly flat at times t_1, t_2, and t_3 (see Figure 5). The first flattening is attributed to the effect of water vapor release and the effect of the vapor stream on the thermocouples. The second flattening, observed around foam onset temperature, T_{FO}, corresponds to feed shrinkage and sintering as the open porosity of the feed closes and porosity significantly decreases. The third flattening, observed around foam maximum temperature, T_{FM}, occurred when the foam started to collapse and convection began to affect the temperature field. The temperature evolutions of A0 and A19 are similar except that the second flattening (related to the compaction of feed at T_{FO}) occurs at a lower temperature for A19, which compacts at a lower temperature than A0.

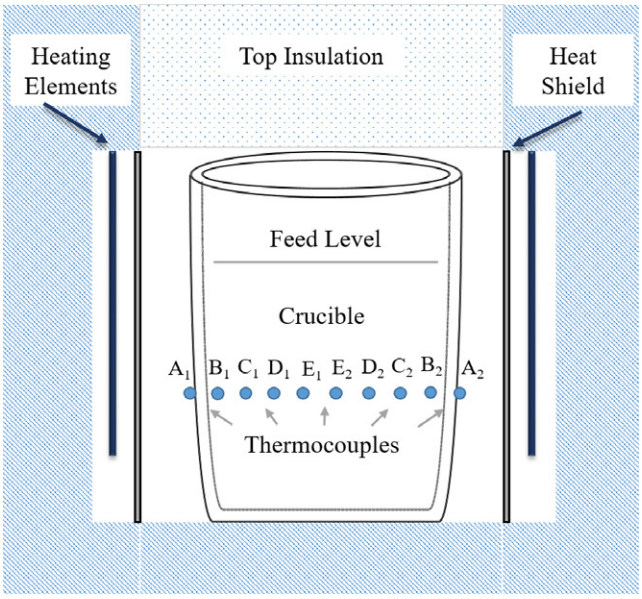

FIGURE 4 Schematic illustration of the furnace setup, showing the position of thermocouples in a fused silica ceramic crucible filled with 465 g of feed

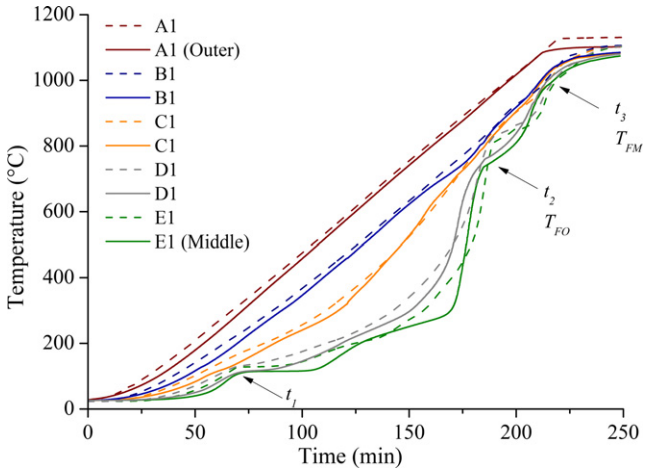

FIGURE 5 Temperatures of feed A0 (dashed lines) and A19 (solid lines) recorded by thermocouples A1–E1, while the crucible was heated at 5 K·min^{-1}. The A1 thermocouple measures the temperature at the outside wall of the crucible, while E1 is located almost in the center of the feed in the crucible

From the measured temperature profiles, the $\lambda(T)$ function of the melter feed was fitted using the FVM together with least-square analysis.[11]

3.4 | Foam morphology from X-ray CT

As reported in Harris et al.[2] the morphology of various feeds during their batch-to-glass transition was investigated using in-situ X-ray computed micro-tomography (μCT, InspeXio SMX-225CT, Shimadzu Co. Ltd., Tokyo, Japan). Pellets made of dry feed, initially cylindrical in shape, were heated at 10 K·min^{-1} and imaged at 20°C intervals from 600°C to 1040°C. Cross sections obtained through central profiles of a pellet and parallel to its axis were digitally segmented into gas and a condensed phase. The primary foam morphology was characterized by the pellet profile area, the maximum bubble diameter, and the void fraction, as displayed in Figure 6 for the A19-5 feed, which has very similar composition to A19. The maximum resolution of the μCT images (cubic voxel with 100 μm edge size) was not sufficient to get information about feed morphology at temperatures below 600°C. However, simultaneous pellet expansion experiments[6] showed that the pellet shape and volume changed little below this temperature. A previous scanning electron microscope analysis showed that the maximum pore size below 700°C was ~30 μm.[8,35,36] This rough value does not affect the results because the contribution of radiation at lower temperatures is negligible.

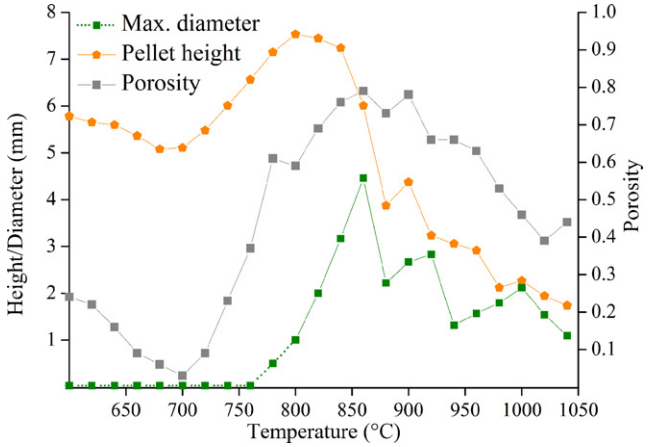

FIGURE 6 Maximum bubble diameter, pellet height, and porosity as functions of temperature, evaluated from μCT images.[2] The dotted green line below 800°C represents values estimated from scanning microscope analysis[8,35,36]

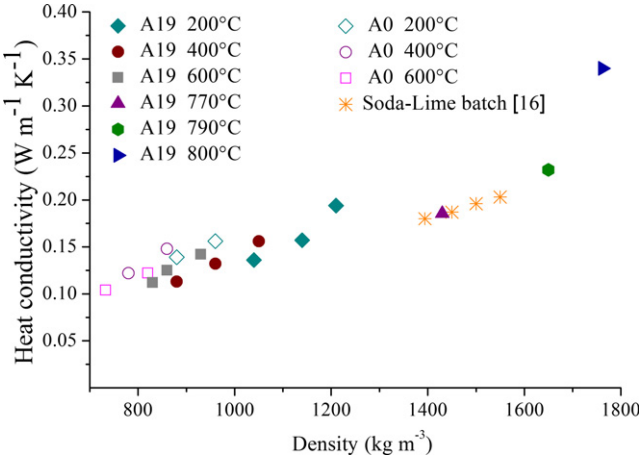

FIGURE 7 Comparison of the heat conductivity A19 and A0 dry feeds as a function of sample density and temperature it was heated to. Literature data for soda-lime-silica batches[16] are also plotted for comparison

4 | RESULTS

4.1 | Heat conductivity of A0 and A19 dry feed using THB 100

Figure 7 displays the results of heat conductivity measurements of A0 and A19 dry powder feeds using a Linseis THB100. The measured heat conductivity depends both on the density of the powder feed (its compaction) and on the temperature to which the feed was heated before the measurement at room temperature was conducted.

The values obtained using the conductivity meter are similar for A19 and A0 dry powder. Moreover, they are in good agreement with literature values on a soda-lime glass batches, obtained by a different method.[16,17] Heat conductivities of samples heated to higher temperatures (700°C, 770°C, 790°C, 800°C) greatly increase with temperature because of the sintering effect and feed shrinkage (see Figure 2B). Visible glass-forming melt appeared above 800°C, associated with the onset of foaming, which prevented us from measuring meaningful λ values at higher temperatures.

Figure 8 compares heat conductivity measured by the THB (points) with that evaluated by FVM (see Rice et al.[11] for details) from the heat penetration experiment performed with A19 (solid lines) and A0 (dashed lines). The λ values for A19 and A0 feeds measured by THB are nearly identical, and are close to values from heat penetration experiments at 200°C[11]. At temperatures above 300°C, the THB and heat penetration values start to deviate. The conductivity measured by THB at room temperature is lower because molten salt recrystallizes upon cooling; between 300°C and 600°C, boric acid and oxyionic salts (nitrates, nitrites, carbonates) react and melt. Molten phase,

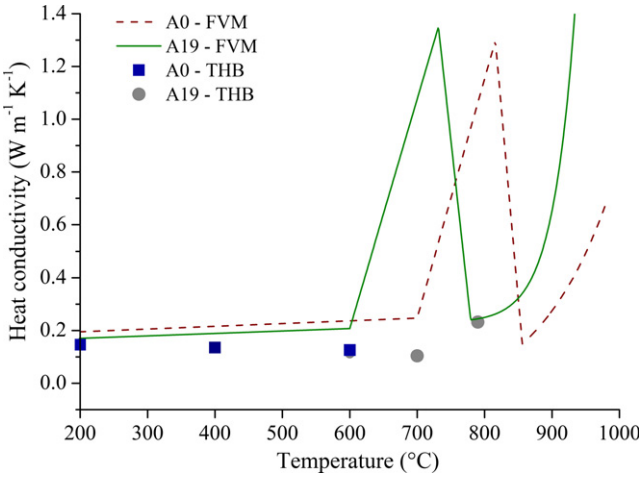

FIGURE 8 Comparison of heat conductivity of A19 and A0 dry feed measured using THB and evaluated from heat penetration experiment by FVM[11]

although present in a small fraction, wets feed particles, enhancing the conductivity.

Above 600°C, λ values go through a maximum at the foam onset temperature T_{FO} (~700°C for A19, ~800°C for A0) related to feed densification. The decrease in $\lambda(T)$ for $T>T_{FO}$ is attributable to the insulating effect of gas in primary foam. Radiative heat transfer in conjunction with the increasing size of foam cells causes the second sharp increase in λ. At this point, the λ values become affected by convection and the growth and collapse of bubbles as the main contributors to heat transfer. The $\lambda(T)$ curves follow similar trends but are shifted by ~100°C. This is caused by earlier formation of glass-forming melt in A19

feed resulting in earlier feed compaction (see the difference in T_{FO} in Figure 5).

The movement of the A19 feed associated with its shrinkage (see Figure 2A,B) starts at the wall when the temperature increases above 600°C and then progresses to the crucible center, possibly even affecting the location of the thermocouples (by bringing them closer together). The radial component of this feed movement affects the temperature field, possibly resulting in higher apparent heat conductivity. Although the real heat conductivity increases as the feed shrinks, feed displacement by shrinkage and primary foam growth result in overestimated λ values. On the other hand, the THB values in this region are likely underestimated, especially due to the crystallization of salts and solidification of the glass-forming melt upon cooling. Thus, it is plausible that the real heat conductivity values are somewhere between the THB and heat penetration values.

The difference between the temperature intervals of A19 feed shrinkage during the THB experiments (700-800°C, see Table 2) and during the heat penetration test (600-700°C) is attributable to the different furnaces and different setups used. Thermocouples were in direct contact with the feed in the heat penetration test, whereas ceramic crucibles were used in the THB test, which could shield the feed during the heating.

4.2 | Heat conductivity of FDSB and cold-cap samples

Next to the dry powder feed, Figure 9 presents heat conductivities of FDSB samples, measured by both THB and HTP sensors together with the range of heat conductivities of the cold-cap samples. The λ values for FDSB samples are considerably higher than those of the dry powders. This is mainly caused by the higher connectivity of the feed in FDSB, which forms a solid block of material. The λ values of FDSB samples decrease as temperature increases. This is mostly caused by gas-evolving reactions, such as release of water from gibbsite,[36] which increase the feed porosity and decrease the connectivity of the feed in the porous block. However, the as-received and 200°C heat-treated FDSB samples were stiff and hard, the gibbsite dehydration at 250-350°C loosened the feed block structure, which was typically accompanied by minor volume expansion (also reported in Lee et al.[6]).

Using an HTP sensor, the heat conductivity values measured for the open-porosity layer in four LSM cold-cap samples[34] were 0.330, 0.275, 0.235, and 0.177 $W \cdot m^{-1} \cdot K^{-1}$. Considering that the temperature of the feed in this layer reached approximately 400°C-600°C,[34] the results are in agreement with measured FDSB values (the gray box in Figure 9), indicating similarity between the cold cap and

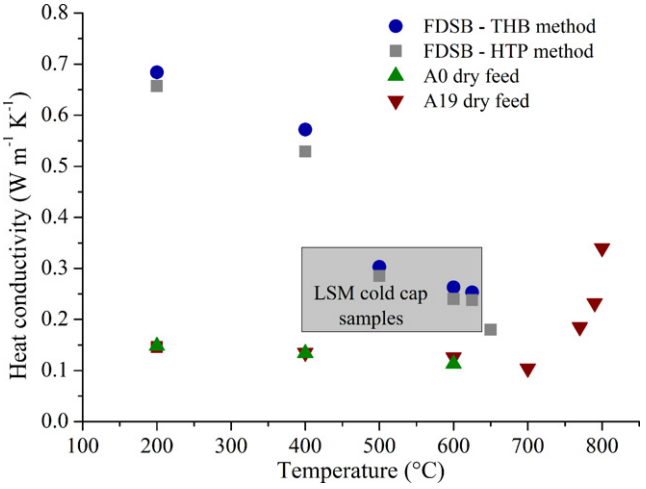

FIGURE 9 The heat conductivity of FDSB and loose dry feed measured by THB and HTP sensors. The gray box shows the range of values measured for cold-cap samples, and illustrates the uncertainty in the temperatures to which the feed in the open-porosity layer was heated in the cold-cap samples

FDSBs. The lowest value was measured for the cold-cap sample heated to the highest temperature, ~550°C, as confirmed by subsequent thermogravimetric analysis of the sample from the cold cap.

As discussed in the previous section, the THB and HTP values can underestimate the real conductivity values because molten salts solidify upon cooling to room temperature.

4.3 | Theoretical prediction of heat conductivity of glass batch

The solid line in Figure 10 displays the effective heat conductivity of a representative feed containing 50% crystalline silica and 50% amorphous material (glass cullet) obtained by Equations 1-5 and porosity and bubble size from Figure 6. Within the temperature interval of 750-1040°C, the dashed line represents an upper boundary of primary-foam heat conductivity, because the maximum equivalent diameter from 2D CT images was used for calculation. The average bubble diameter will be used once a full 3D analysis of the X-ray data become available.

To fit the λ values obtained by FVM, Ψ=0.58 was used for the feed connectivity in Equation 5. This is a considerably higher value than that measured for the silica sand batch (Ψ=0.29). As the parameter Ψ can be regarded as a measure for the heat transfer area between the particles in the batch, this suggests significantly larger contact area between the particles in the A19 feed. The true Ψ value would likely also increase when the feed densifies and eventually turns into melt, thus increasing λ.

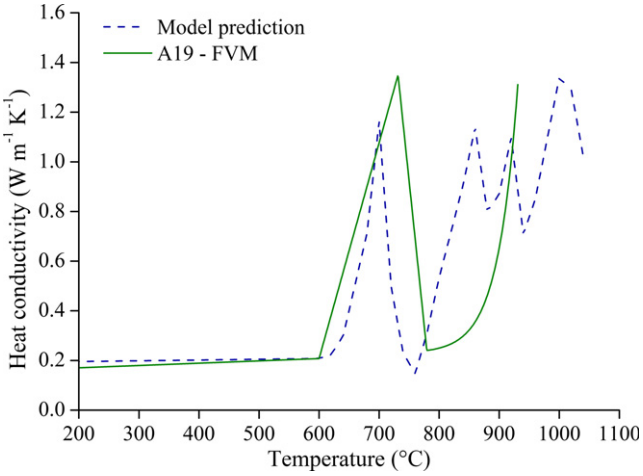

FIGURE 10 Comparison of theoretically predicted and measured dependence of heat conductivity on temperature

Estimated and experimental $\lambda(T)$ trends are in reasonable agreement (Figure 10). The $\lambda(T)$ functions are nearly constant at T<600°C, sharply increase in the ~600°C-700°C interval as the feed densifies (see Figure 6), abruptly drop in a ~50°C interval as the melt turns into foam with small pores, and increase again as larger bubbles form, permitting increased radiative transfer (Equation 4). For the model prediction, λ then oscillates as bubbles burst (see Figure 6), and finally reaches values expected for bubble-free glass (~1-1.5 $W \cdot m^{-1} \cdot K^{-1}$).[11,37]

The estimated values are generally slightly lower than values evaluated from the heat penetration experiment. At temperatures below ~600°C, this is possibly caused by the formation of a small amount of molten phase in the feed. Above 600°C, this is likely caused by the movement of the feed during its shrinkage and foaming, which results in overestimation of λ from the heat penetration tests.

The result displayed in Figure 10 is valid for a single feed measured at a single heating rate, its main purpose is to show the predictive ability of the heat transfer model. Currently, this model is being coupled with kinetic models of the batch-to-glass transition, which describe porosities of various feeds as a function of heating rate (time-temperature history). Moreover, the heat transfer model will be used once the results of in-situ X-Ray tomography of a cold cap during melting in a LSM become available.

5 | DISCUSSION

As mentioned in the introduction, the goal of this study is to determine the temperature-dependent heat conductivity for the mathematical model of a cold cap. As explained in our previous work,[11,13] λ influences the rate of melting via a complex interdependence of heat transfer and feed-to-glass conversion kinetics. In this work, we found that the heat conductivity of the feed formed in the cold cap at temperatures below T_{FO} is considerably higher than the heat conductivity of a dry powder feed, which is typically used for laboratory crucible experiments. This has a significant consequence for model predictions, as higher λ values lead to better heat transfer and thus faster melting in the cold cap. This more realistic value will be used for the modeling of the batch-to-glass conversion in the cold cap.

Above T_{FO}, when primary melt evolves and feed turns into foam, primary foam expansion and melt convection significantly complicate the evaluation of λ. Moreover, it is impossible to directly measure the heat conductivity of gas cavities, which are formed by the collapsing primary foam and by the secondary foam bubbles formed in the molten glass. However, the presented theoretical approach for the estimation of λ, which is based on equations for multiphase heat transfer (including radiation) and in-situ X-ray morphology data, gives us a powerful tool to assess heat transfer through primary foam and cavities.

A remaining minor issue is that the THB and HTP values might somewhat underestimate the real conductivity values because molten salts solidify upon cooling to room temperature. If more precise data are needed, a heat penetration experiment with FDSB could be performed, which would, however, require the thermocouples to be immersed in the feed during the FDSB fast drying preparation process.

6 | CONCLUSIONS

To assess the heat conductivity, λ, of a melter feed in the cold cap, we prepared FDSBs by imitating actual conditions during the cold-cap formation in a melter. Using a heat conductivity meter, we found that λ of such cold-cap-like samples is considerably higher than the heat conductivity of the dry powder feed. The reason for this is a significantly higher connectivity of the feed in the cold cap, which, after the fast water evaporation from slurry, creates a solid block of material. These results were confirmed by measuring the heat conductivity of cold-cap samples retrieved from an LSM, which corresponded well to λ of FDSBs.

To the best of our knowledge, this paper also presents the first attempt to estimate the heat conductivity of primary foam using in-situ X-ray computed tomography. Our comparison of the estimated and measured λ provides convincing evidence that this model could also be useful for the assessment of heat transfer in cavities and in secondary foam, for which it is impracticable to measure λ experimentally. We believe that the combination of heat transfer modeling and in-situ X-ray tomography opens a novel approach to mathematical modeling

of batch-to-glass conversion in both waste and commercial glass melters.

ACKNOWLEDGMENT

This work was supported by the U.S. Department of Energy's Waste Treatment & Immobilization Plant Project of the Office of River Protection under the direction of Albert A. Kruger. Pacific Northwest National Laboratory is operated for the Department of Energy by Battelle Memorial Institute under contract DE-AC05-76RL01830. Miroslava Hujova acknowledges financial support from specific university research (MSMT No 20-SVV/2017).

REFERENCES

1. Kirkbride RA. Tank waste remediation system operation and utilization plan, Vol. 1 HNF SD-WM-SP-012. Richland, WA: Numatec Hanford Corporation; 1997.
2. Harris WH, Guillen DP, Kloužek J, et al. X-ray tomography of feed-to-glass transition of simulated borosilicate waste glass. *J Am Ceram Soc*. 2017;1-12. https://doi.org/10.1111/jace.14895.
3. Kim D, Schweiger MJ, Buchmiller WC, Matyas J. Laboratory-Scale Melter for Determination of Melting Rate of Waste Glass Feeds Richland, WA: PNNL-21005; EMSP-RPT-012, Pacific Northwest National Laboratory; 2015.
4. Pokorny R, Pierce DA, Hrma P. Melting of glass batch: Model for multiple overlapping gas-evolving reactions. *Thermochim Acta*. 2012;541:8-14.
5. Chun J, Pierce DA, Pokorný R, et al. Cold-cap reactions in vitrification of nuclear waste glass: Experiments and modeling. *Thermochim Acta*. 2013;559:32-39.
6. Lee S, VanderVeer BJ, Hrma P, et al. Effects of heating rate, quartz particle size, viscosity, and form of glass additives on high-level waste melter feed volume expansion. *J Am Ceram Soc*. 2017;100:583-591.
7. Hrma P, Schweiger MJ, Humrickhouse CJ, et al. Effect of glass-batch makeup on the melting process. *Ceram - Silik*. 2010;54: 193-211.
8. Pierce DA, Hrma P, Marcial J, et al. Effect of alumina source on the rate of melting demonstrated with nuclear waste glass batch. *Int J App Glass Sci*. 2012;3:59-68.
9. Schweiger MJ, Hrma P, Humrickhouse CJ, et al. Cluster formation of silica particles in glass batches during melting. *J Non-Crys Sol*. 2010;356:1359-1367.
10. Pokorny R, Rice JA, Crum JV, et al. Kinetic model for quartz and spinel dissolution during melting of high-level-waste glass batch. *J Nucl Mater*. 2013;443:230-235.
11. Rice J, Pokorny R, Schweiger M, et al. Determination of heat conductivity and thermal diffusivity of waste glass melter feed: extension to high temperatures. *J Am Cer Soc*. 2014;97:1952-1958.
12. Pokorny R, Hilliard ZJ, Dixon DR, et al. One-dimensional cold cap model for melters with bubblers. *J Am Cer Soc*. 2015;98: 3112-3118.
13. Pokorny R, Rice JA, Schweiger MJ, et al. Determination of temperature-dependent heat conductivity and thermal diffusivity of waste glass melter feed. *J Am Cer Soc*. 2013;96:1891-1898.
14. Faber AJ, Beerkens RGC, Waal HD. Thermal behaviour of glass batch on batch heating. *Glastech Ber*. 1992;7:177-185.
15. Conradt R, Suwannathada P, Pimkhaokam P. Local Temperature distribution and primary melt formation in a melting batch heap. *Glastech Ber*. 1994;67:103-113.
16. Verheijen OS. Thermal and chemical behavior of glass forming batches. PhD thesis. Technische Universiteit Eindhoven, TU Eindhoven, ISBN 90-386-2555-3, 2003.
17. Verheijen OS, Op den Camp OMGC, Beerkens RGC. Heating of glass-forming batch blankets. In: *63rd Conference on Glass Problems: Ceramic Engineering and Science Proceedings*. Vol 24. Westerville, OH: The American Ceramic Society; 2008;101-114.
18. Pokorny R, Kruger A, Hrma P. Modeling of cold cap: effect of bubbling on melting rate. *Ceram - Silik*. 2014;58:296-302.
19. Hammerschmidt U, Meier V. New transient hot-bridge sensor to measure thermal conductivity, thermal diffusivity, and volumetric specific heat. *Int J Thermophys*. 2006;27:840-865.
20. Wang M, Pan N. Predictions of effective physical properties of complex multiphase materials. *Mater Sci Eng R: Rep*. 2008;63:1-30.
21. Loeb AL. Thermal conductivity: VIII, a theory of thermal conductivity of porous materials. *J Am Ceram Soc*. 1954;37:96-99.
22. Bouguerra A. Prediction of effective thermal conductivity of moist wood concrete. *J Phys D: App Phys*. 1999;32:1407-1414.
23. Alharthi A, Lange J. Soil water saturation: dielectric determination. *Water Resour Res*. 1987;23:591-595.
24. Cosenza P, Guerin R, Tabbagh A. Relationship between thermal conductivity and water content of soils using numerical modelling. *Eur J Soil Sci*. 2003;54:581-588.
25. Ferkl P, Pokorny R, Bobák M, et al. Heat transfer in one-dimensional micro- and nano-cellular foams. *Chem Eng Sci*. 2013;97:50-58.
26. Ferkl P, Pokorny R, Kosek J. Multiphase approach to coupled conduction–radiation heat transfer in reconstructed polymeric foams. *Int J Therm Sci*. 2014;83:68-79.
27. Meisterova L, Zubov A, SmolnA K, et al. X-ray tomography imaging of porous polyolefin particles in an electron microscope. *Macrom React Eng*. 2013;7:277-288.
28. Mann D, Field RE, Viskanta R. Determination of specific heat and true thermal conductivity of glass from dynamic temperature data. *Wärme- und Stoffübertragung*. 1992;27:225-231.
29. Wakao N, Kaguei S. Topics in chemical engineering. *Heat and mass transfer in packed beds*. Vol 1, 1st edition. New York, NY: Gordon and Breach, Science Publishers, Inc.;1982. ISBN: 0-677-05860-8.
30. Viskanta R, Wu X. Effect of gas percolation on melting of glass batch. *J Am Ceram Soc*. 1984;67:376-380.
31. Pilon L, Viskanta R. Radiation characteristics of glass containing gas bubbles. *J Am Ceram Soc*. 2003;86:1313-1320.
32. Dombrovsky L, Randrianalisoa J, Baillis D, et al. Use of Mie theory to analyze experimental data to identify infrared properties of fused quartzcontaining bubbles. *App Opt*. 2005;44: 7021-7031.
33. Matlack KS, Gan H, Chaudhuri M, et al. DM100 and DM1200 Melter Testing with High Waste Loading Glass Formulations for Hanford High-Aluminum HLW Streams, VSL-10R1690-1; 2010.
34. Dixon DR, Schweiger MJ, Riley BJ, et al. Temperature distribution within a cold cap during nuclear waste vitrification. *Environ Sci & Tech*. 2015;49:8856-8863.

35. Xu K, Hrma P, Rice J, et al. Melter feed reactions at T≤700°C for nuclear waste vitrification. *J Am Ceram Soc*. 2015;98:3105-3111.
36. Xu K, Hrma P, Rice JA, et al. Conversion of nuclear waste to molten glass: cold-cap reactions in crucible tests. *J Am Ceram Soc*. 2016;99:1-7.
37. Rodriguez CP, Chun J, Crum JV, et al. Thermal properties of simulated Hanford waste glasses. *J Am Ceram Soc*. 2017;00:1-10.

How to cite this article: Hujova M, Pokorny R, Klouzek J, et al. Determination of heat conductivity of waste glass feed and its applicability for modeling the batch-to-glass conversion. *J Am Ceram Soc*. 2017;00:1–11. https://doi.org/10.1111/jace.15052